Chinese Chemical Letters 37 (2026) 112618

Contents lists available at ScienceDirect

Chinese Chemical Letters

journal homepage: www.elsevier.com/locate/cclet

# Phenylethynyl-bridged naphthalimide probe for super-resolution imaging and polarity decoding of lipid droplets

Jie Pan[a], Shurui Hu[a,b], Wenchao Jiang[a], Junyu Xiao[a], Xiaogang Liu[c], Qinglong Qiao[a,b,*], Zhaochao Xu[a,b,*]

[a] State Key Laboratory of Molecular Reaction Dynamics, Dalian Institute of Chemical Physics, Chinese Academy of Sciences, Dalian 116023, China
[b] University of Chinese Academy of Sciences, Beijing 100049, China
[c] School of Chemistry, Chemical Engineering and Biotechnology, Nanyang Technological University, Singapore 637371, Singapore

ARTICLE INFO

*Article history:*
Received 8 March 2026
Revised 11 March 2026
Accepted 12 March 2026
Available online 13 March 2026

*Keywords:*
Lipid droplets
Fluorescent probe
Polarity
Solvatochromic
Super-resolution imaging

ABSTRACT

Lipid droplets (LDs) serve as central hubs for lipid synthesis, storage, and mobilization, with their biological functions largely governed by the composition of neutral lipid cores. Although *in situ* probing of LD polarity has emerged as a promising strategy to decode compositional remodeling, probes capable of resolving the subtle and narrowly distributed polarity variations within LD interiors remain scarce. Here we report a phenylethynyl-bridged naphthalimide probe (TS-N) that enables sensitive decoding of LD polarity in living cells. Introduction of a conjugated phenylethynyl spacer significantly increases the intramolecular charge-transfer distance ($d_{CT} = 3.561$ Å), resulting in enhanced solvatochromic responsiveness with an emission shift exceeding 220 nm across solvent polarity gradients. The probe exhibits a high polarity sensitivity of 14.5 nm per unit, enabling detection of subtle dielectric variations within weakly polar LD interiors. TS-N selectively targets LDs and supports long-term super-resolution imaging of dynamic processes, including LD fusion and mitochondria-LD interactions. Importantly, quantitative *in situ* fluorescence spectral analysis reveals that TS-N can resolve metabolic perturbation-induced polarity fluctuations at the single-droplet level and correlate dielectric changes with droplet size remodeling. This strategy integrates structural imaging with compositional decoding, providing a powerful tool for investigating LD metabolic heterogeneity and organelle interactions in living cells.

© 2026 Published by Elsevier B.V. on behalf of Chinese Chemical Society and Institute of Materia Medica, Chinese Academy of Medical Sciences.

Lipid droplets (LDs) are ubiquitous and highly dynamic intracellular organelles that function as central hubs for lipid synthesis [1], storage [2–4], and mobilization. Beyond serving as inert lipid depots, LDs actively participate in cellular energy homeostasis, stress adaptation, signaling regulation, and organelle communication [5–8]. The functional state of LDs is fundamentally dictated by compositional remodeling within their neutral lipid core, primarily composed of triacylglycerols (TAGs) and cholesteryl esters (CEs) [9,10]. Variations in lipid species, degrees of unsaturation, and oxidative modification accompany metabolic reprogramming, lipotoxic stress, and cell fate transitions [11]. Notably, the CE/TAG ratio has emerged as an important indicator for disease staging and prognosis, further highlighting the pathological relevance of LD compositional dynamics [12,13]. These compositional changes also directly reflect shifts in lipid metabolic flux and organelle function, underscoring the importance of resolving LD composition *in situ* and in real time [14–16].

Traditionally, LD compositional analysis relies on liquid chromatography–tandem mass spectrometry (LC–MS/MS)-based lipidomics [17–19], which enables highly accurate quantification of purified lipid extracts at cellular or tissue levels and precise identification of individual molecular species. However, such approaches are destructive and endpoint measurements, making it difficult to capture dynamic metabolic remodeling in living cells. More importantly, lipidomics provides population-averaged information, whereas a single cell may contain tens to hundreds of LDs with potential heterogeneity [20]. Consequently, compositional and physicochemical variations within individual LDs remain largely inaccessible. Fluorescence imaging offers a noninvasive strategy to visualize LD structure and dynamics under physiological conditions [21–24]. In particular, super-resolution techniques allow nanoscale visualization of LD fusion, lipophagy, and inter-organelle interactions. Classical LD dyes, including boron-dipyrromethene (BODIPY) 493 and Nile Red [25–27], have realized quantification

* Corresponding authors.
*E-mail addresses:* qqlqiao@dicp.ac.cn (Q. Qiao), zcxu@dicp.ac.cn (Z. Xu).

https://doi.org/10.1016/j.cclet.2026.112618
1001-8417/© 2026 Published by Elsevier B.V. on behalf of Chinese Chemical Society and Institute of Materia Medica, Chinese Academy of Medical Sciences.

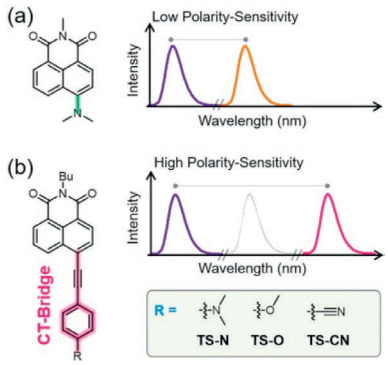



**Fig. 1.** (a) Conventional ICT dyes exhibiting limited polarity sensitivity. (b) Phenylethynyl-bridged design acting as an efficient charge-transfer pathway to significantly enhance polarity sensitivity.

of LD number, size, and morphology [28–32]. However, these probes primarily report structural features and provide limited insight into real-time compositional remodeling within individual droplets, thereby restricting functional interrogation of LD metabolic heterogeneity.

Microenvironmental polarity is intrinsically governed by molecular composition. Therefore, LD polarity serves as a physicochemical surrogate for internal lipid remodeling. Lipid exchange, oxidation, and saturation changes during metabolic perturbation or mitochondria-LD interactions generate subtle dielectric variations within the LD core. Thus, spatiotemporal mapping of LD polarity offers an indirect yet powerful strategy to decode compositional dynamics and associated biological functions [33–38]. However, the LD interior presents a unique challenge that it is uniformly weakly polar and lacks hydrogen-bonding interactions, resulting in a compressed polarity window. Even substantial compositional remodeling produces only minor dielectric changes. Conventional solvatochromic fluorophores, which typically rely on strong intramolecular charge transfer (ICT) responses triggered by large polarity gradients or hydrogen bonding (Fig. 1a), exhibit attenuated or indistinguishable emission shifts under these conditions [39–42]. Therefore, probes capable of resolving small polarity differences with high sensitivity in weakly polar environments are urgently needed.

Here, we introduce a phenylethynyl-bridged naphthalimide probe (TS-N) that achieves enhanced solvatochromic responsiveness (Fig. 1b). By inserting a conjugated phenylethynyl spacer between the electron-donating amino group and naphthalimide acceptor core, the charge-transfer distance ($d_{CT} = 3.561$ Å) is increased to approximately 2.5-fold relative to the non-bridged analogue, thereby amplifying polarity sensitivity. TS-N exhibits an emission shift spanning over 220 nm across solvent polarity gradients, with a relative polarity-dependent emission shift rate of 14.5 nm, enabling high-resolution decoding of subtle dielectric variations. Importantly, TS-N can precisely target LDs and enable super-resolution imaging of LD dynamic processes, including fusion events and mitochondria-LD interactions. Quantitative *in situ* analysis demonstrates that TS-N can resolve metabolic perturbation-induced polarity fluctuations at the single-droplet level while correlating dielectric changes with droplet size remodeling. This probe holds strong potential to integrate structural imaging with compositional decoding, thereby enabling functional interrogation of LD metabolic heterogeneity in living cells.

We first investigated the photophysical properties of the phenylethynyl-bridged derivatives. Both TS-O and TS-N exhibited pronounced solvatochromic behavior in different solvents (Figs. 2a and b, Figs. S1-S3 in Supporting information). Notably, TS-N displayed an exceptionally large emission shift spanning over 220 nm across the solvent series, with maximum $\lambda_{em}$ located at 513 nm in hexane and red-shifted to 736 nm in methanol (Fig. 2c). In contrast, its absorption spectra remained nearly unchanged in different solvents, indicating that the polarity response predominantly arises from excited-state modulation rather than ground-state perturbation. By comparison, the electron-deficient derivative TS-CN showed minimal polarity responsiveness, with almost invariant fluorescence emission across solvents, confirming the essential role of the donor–acceptor framework in enabling solvatochromism (Fig. S4 in Supporting information). We also evaluated Nile Red and a reference naphthalimide derivative lacking the phenylethynyl bridge (4-dimethylamino-1,8-naphthalimide (DMN)) under identical solvent conditions (Figs. S5 and S6 in Supporting information). For quantitative comparison, we calculated the average emission shift per solvent polarity increment. TS-N and TS-O exhibited sensitivity values of 14.5 nm and 7.0 nm, respectively, whereas Nile Red displayed only 4.4 nm and DMN merely 3.5 nm (Fig. 2d and Fig. S7 in Supporting information). These results clearly demonstrate that incorporation of the phenylethynyl bridge dramatically enhances polarity responsiveness, endowing TS-N and TS-O with superior capability for detecting subtle dielectric variations.

To elucidate the origin of the enhanced polarity sensitivity, we calculated the charge redistribution between the ground and excited states using DMN as the reference structure (Fig. 2e). The degree of ICT was quantified using the charge transfer distance ($d_{CT}$), defined as the spatial separation between the barycenters of positive ($\Delta\rho^+$) and negative ($\Delta\rho^-$) electron density increments upon excitation [43]. The calculated $d_{CT}$ value for TS-N (3.561 Å) was approximately 2.5 times larger than that of DMN (1.438 Å), indicating a significantly enhanced ICT character in the $S_1$ state of TS-N. This value was also considerably larger than those reported for Nile Red (0.946 Å) and BODIPY dyes (0.445 Å) [44]. Furthermore, TS-N exhibited a substantially higher oscillator strength ($f$) than the reference compound, corresponding to enhanced absorption capability. This theoretical prediction agreed well with experimental data that TS-N showed a molar extinction coefficient of ~25,000 L mol$^{-1}$ cm$^{-1}$, nearly double that of DMN (~12,000 L mol$^{-1}$ cm$^{-1}$). Compared with TS-O and TS-CN, TS-N displays larger $d_{CT}$ and $f$ values, further confirming that the phenylethynyl unit functioned as an efficient charge-transfer bridge that increases the donor–acceptor separation and amplifies excited-state polarization. The resulting enhanced charge-transfer character increased the dielectric sensitivity of the excited state, thereby leading to a more pronounced emission response to polarity variations.

To further quantify polarity-related electronic redistribution, we evaluated the molecular polarity index (MPI) [45], derived from the surface electrostatic potential distribution (Fig. 2f). Although TS-N showed a relatively lower MPI in the ground state (13.2 kcal/mol) than DMN, its excited-state MPI markedly increased to 27.4 kcal/mol, surpassing that of DMN (23.0 kcal/mol). This substantial excited-state polarity amplification further explained the pronounced solvatochromic behavior of TS-N and confirms that phenylethynyl-mediated conjugation engineering enhanced sensitivity to subtle environmental polarity changes. Such characteristics made TS-N particularly suitable for probing weakly polar microenvironments with narrow dielectric variation ranges.

We then assessed the LD targeting capability of TS-N in live cells. Colocalization experiments were performed using our previously reported probe LD 688P (Figs. 3a and b) [46]. TS-N displayed specific accumulation within LDs, exhibiting a Pearson's correlation coefficient exceeding 0.88 with LD 688P, thereby confirming its excellent LD selectivity (Fig. S8 in Supporting information). For long-term visualization of LD dynamics, high photostability is essential. Environment-sensitive fluorophores frequently suffer from rapid photobleaching, as extended and flexible $\pi$-conjugated

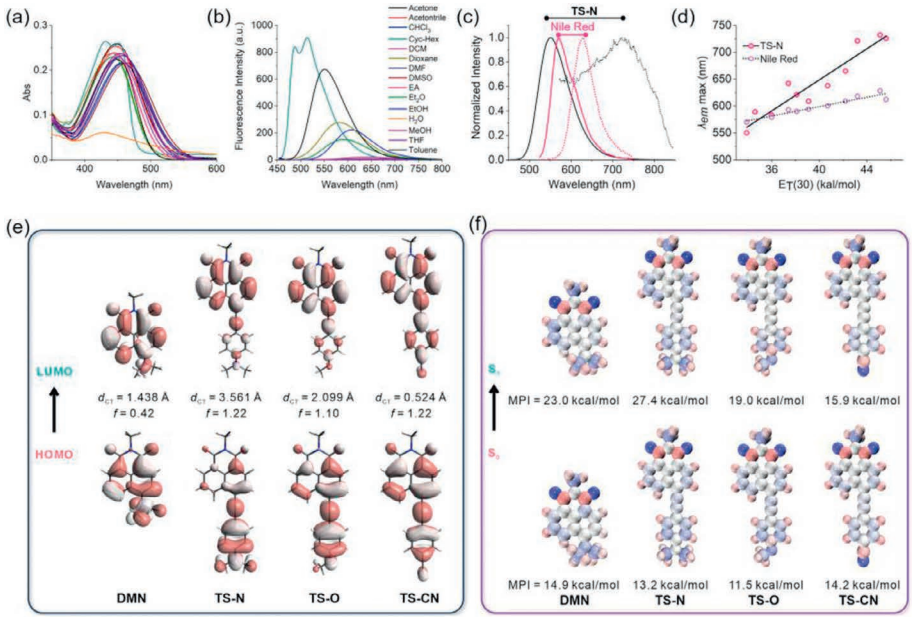



**Fig. 2.** The absorption (a) and fluorescence spectra (b) of TS-N in various solvents. (c) Fluorescence spectra of TS-N and Nile Red in toluene (solid line) and DMSO (dotted line). (d) Plot of the emission wavelength maximum of TS-N and Nile Red in different solvents *vs.* $E_T$ (30). (e) Highest occupied molecular orbital (HOMO) and lowest unoccupied molecular orbital (LUMO) distributions of the dyes, together with the charge-transfer distance ($d_{CT}$) obtained from electron-hole analysis and the *f*. (f) MPI values of the dyes. Atomic dipole moment corrected Hirshfeld (ADCH) charge distributions in the $S_0$ and $S_1$ states are also shown for reference.

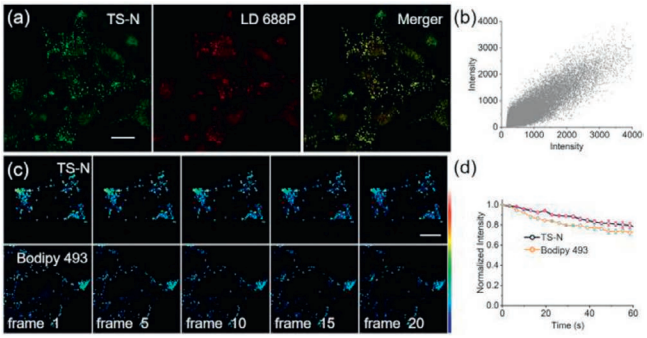



**Fig. 3.** (a) Confocal fluorescence images of live HeLa cells co-stained with TS-N and LD 688P (1.0 μmol/L). Scale bar: 20 μm. (b) Intensity correlation plot of dyes TS-N and LD 688P. (c) Time-lapse confocal images of LDs stained with TS-N or BODIPY 493 (1.0 μmol/L) under continuous 488 nm laser irradiation for 60 s. Scale bar: 10 μm. (d) Relative fluorescence intensity changes of enlarged region in living HeLa cells.

systems are prone to singlet oxygen-mediated oxidative degradation under continuous irradiation. Given that TS-N incorporates a phenylethynyl spacer between the amino donor and the naphthalimide acceptor, we anticipated that the increased structural rigidity and extended conjugation would enhance photostability by reducing conformational flexibility. To evaluate this hypothesis, we examined the photostability of TS-N under confocal imaging by repeatedly acquiring fluorescence images from the identical cellular region under continuous 488 nm excitation (Fig. 3c). For comparison, the commercial LD dye BODIPY 493 was tested under identical conditions (Fig. 3d). HeLa cells were incubated with TS-N (2 μmol/L) for 0.5 h prior to imaging. Upon continuous irradiation, TS-N retained over 83 % of its initial fluorescence intensity, whereas BODIPY 493 exhibited faster photobleaching, with intensity decreasing to below 70 %. Such enhanced photostability provided a reliable foundation for capturing LD fusion, morphological remodeling, and organelle interactions in living cells. Notably, TS-O also demonstrated precise LD localization in live cells (Fig. S9 in Supporting information), highlighting the general applicability of this phenylethynyl-engineered design strategy for LD targeting.

Leveraging its high photostability and enhanced environmental sensitivity, TS-N was employed for long-term super-resolution imaging of LD dynamics in living cells. In LD-enriched regions, multiple fusion events were observed within the first 10 min (Fig. 4a, white arrows), with fusion occurring frequently during this initial period (Fig. 4b). Interestingly, although small LDs-presumably characterized by higher surface tension-remained in close proximity thereafter, no additional fusion events were detected during the subsequent 30 min.

Notably, we captured a complete LD fusion and subsequent morphological relaxation process. Between 540 s and 640 s, two adjacent LDs underwent coalescence (Fig. 4c), forming a newly generated LD with an irregular morphology. Merging super-resolution images at 640 s and 660 s revealed a contracted green region (dotted frame), demonstrating gradual morphological relaxation. This fusion-induced rounding process was consistent with surface tension-driven minimization of interfacial free energy, whereby the newly formed droplet might undergo shape relaxation to reach a thermodynamically favorable spherical configuration.

Long-term super-resolution imaging further enabled visualization of dynamic mitochondria-LD interactions (Figs. 4d and e), revealing both sustained and transient contacts at the nanoscale. In one example, the LD indicated by the white arrow maintained tight contact with mitochondria for over 8 min, suggesting prolonged metabolic coupling. In another instance, a mitochondrion extended a protrusion toward a neighboring LD at 260 s (blue arrow), followed by gradual retraction at 360 s, representing typical transient contact. Additional observations revealed an LD, labelled with orange arrow, serving as a nodal point for three linear mitochondria, with simultaneous interactions occurring between 40 s and 80 s. In certain cases, LDs appeared partially wrapped by mitochondria (Fig. 4e, white arrow), which was further confirmed by intensity profile analysis (Figs. 4f and g). Furthermore, the orange-labeled LD gradually migrated toward the center of a ring-like mitochondrial network at 180 s, potentially increasing contact area and facilitating lipid transfer. These observations highlight the heterogeneous

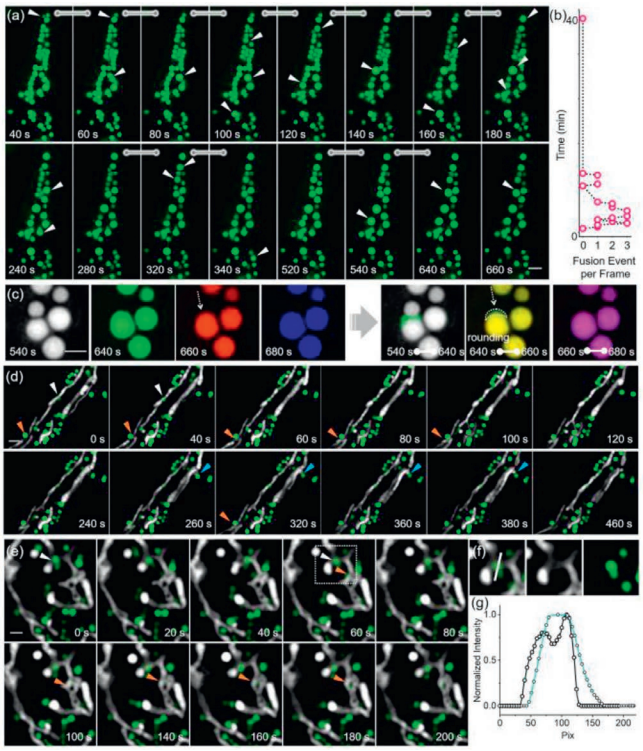


**Fig. 4.** (a) Structured illumination microscopy (SIM) images of living HeLa cells stained with TS-N showing dynamic LD coalescence. Scale bar: 1 μm. (b) Number of LD fusion events occurring every 20 s within 40 min in panel (a). (c) SIM images of LDs during 540–680 s. Images at different time points are pseudo-colored as white, green, red, and blue. Overlay images at 540/640 s, 640/660 s, and 660/680 s illustrate the morphological changes of LDs before and after fusion. Scale bar: 1 μm. (d, e) SIM images of living HeLa cells co-stained with TS-N and MitoTracker Red to visualize interactions between LDs and mitochondria. Scale bar: 1 μm. (f) Enlarged SIM image of mitochondria and LDs in the region of interest (ROI) of panel (e) at 60 s. (g) Fluorescence intensity profile along the line across the mitochondrion and LD in panel (f).

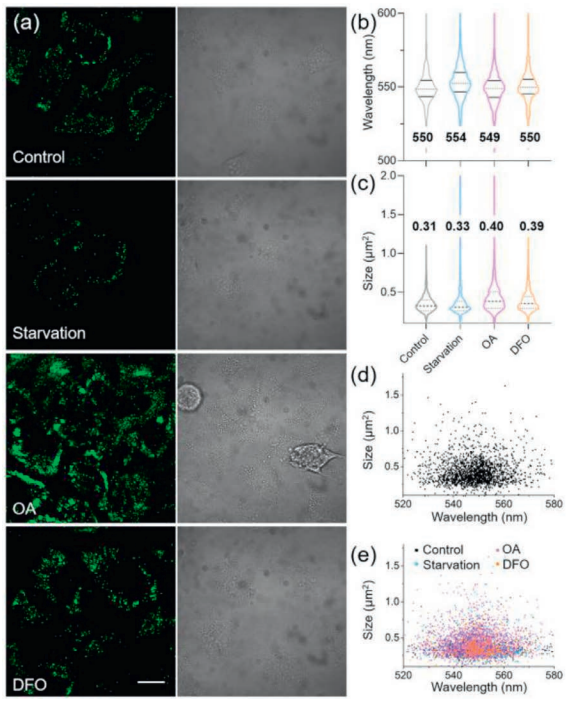


**Fig. 5.** (a) Confocal imaging of live HeLa cells stained with TS-N under different treatments, including starvation, OA, and DFO. Scale bar: 20 μm. (b) Average maximum emission wavelength and (c) LD size of LDs under different conditions. Correlation between LD size and polarity in HeLa cells treated with OA (d) and other stimuli (e).

and dynamic nature of mitochondria-LD interactions and underscore the ability of TS-N to resolve nanoscale organelle crosstalk in real time.

To assess the capability of TS-N in reporting real-time LD polarity changes, cells were subjected to starvation, oleic acid (OA) supplementation, and deferoxamine (DFO) treatment (Fig. 5a). Starvation significantly reduced LD numbers, whereas OA supplementation increased LD abundance. DFO-treated cells maintained LD numbers comparable to control group. *In situ* fluorescence spectral analysis of >600 LDs per group revealed that starvation slightly increased LD polarity, with the average emission wavelength red-shifting from 550 nm (control) to 554 nm, accompanied by a modest size increase from 0.31 μm$^2$ to 0.33 μm$^2$ (Figs. 5b and c). Here, LD size was quantified using projected 2D area. In contrast, OA treatment resulted in substantial LD enlargement (0.40 μm$^2$) with only a minor polarity decrease (549 nm), consistent with neutral lipid accumulation and increased hydrophobicity. Similarly, DFO treatment induced LD enlargement (0.39 μm$^2$) while maintaining polarity levels close to control group, suggesting lipid accumulation with reduced oxidative modification. Correlation analysis between LD size and polarity (Figs. 5d and e) revealed pronounced heterogeneity in control cells (0.2–0.6 μm$^2$). OA-treated cells exhibited increased dispersion and reduced uniformity. In contrast, LDs in DFO-treated cells appeared more homogeneous and tightly distributed, possibly due to suppression of lipid peroxidation and reduced compositional variability within the droplets. Collectively, these results demonstrate that TS-N not only resolves subtle polarity fluctuations within individual LDs but also simultaneously enables super-resolution visualization of LD morphological remodeling and organelle interactions, providing a powerful tool for functional interrogation of lipid metabolic heterogeneity in living cells.

In conclusion, we had developed a phenylethynyl-bridged naphthalimide probe (TS-N) that enables sensitive visualization of LD polarity and morphological dynamics in living cells. Incorporation of a conjugated phenylethynyl spacer between the donor and acceptor units significantly extends the intramolecular charge-transfer distance, resulting in enhanced excited-state polarization and amplified solvatochromic responsiveness. Consequently, TS-N exhibits a large emission shift across solvent polarity gradients and high polarity sensitivity, enabling detection of subtle dielectric variations within the weakly polar interiors of LDs. In addition, TS-N displays excellent LD selectivity and high photostability, supporting long-term super-resolution imaging of LD dynamic processes, including droplet fusion, morphological relaxation, and mitochondria-LD interactions. *In situ* fluorescence spectra further demonstrate that TS-N can resolve metabolic perturbation-induced polarity fluctuations at the single-droplet level and uncover correlations between droplet polarity and size remodeling under different metabolic conditions. The phenylethynyl-bridged design strategy presented here provides a general framework for developing highly sensitive probes for weakly polar biological microenvironments, thereby facilitating mechanistic investigations of lipid metabolism, organelle communication, and metabolic heterogeneity in living cells.

## CRediT authorship contribution statement

**Jie Pan:** Writing – original draft, Investigation, Data curation. **Shurui Hu:** Investigation, Data curation. **Wenchao Jiang:** Data curation. **Junyu Xiao:** Data curation. **Xiaogang Liu:** Investigation, Data curation. **Qinglong Qiao:** Writing – review & editing, Writ-

ing – original draft, Supervision, Investigation, Funding acquisition. **Zhaochao Xu:** Writing – review & editing, Supervision, Funding acquisition.

## Declaration of competing interests

The authors declare that they have no known competing financial interests or personal relationships that could have appeared to influence the work reported in this paper.

## Acknowledgments

This work is supported by the National Natural Science Foundation of China (Nos. 22225806, 22522816, 22578443, 22378385, 22278394, 22507121, 22508383, 22541705, U25A20620); The Chinese Academy of Sciences Project for Young Scientists in Basic Research (No. YSBR-104); The Energy Revolution S&T Program of Yulin Innovation Institute of Clean Energy (No. E412050705); Liaoning Binhai Laboratory (No. LBLD-2024-07); Dalian Institute of Chemical Physics (Nos. DICP I202436, DICP I202522, DICP I202512, DICP&SIA UN202502, DMU-1&DICP UN202301, DMU-1&DICP UN202302, DMU-2&DICP UN202502); Natural Science Foundation of Liaoning (Nos. 2025-MS-061, 2025-BS-0147); Dalian Science and Technology Innovation Fund Program (No. 2022JJ11CG007).

## Supplementary materials

Supplementary material associated with this article can be found, in the online version, at doi:10.1016/j.cclet.2026.112618.

## References

[1] A.R. Thiam, R.V. Farese Jr, T.C. Walther, Nat. Rev. Mol. Cell Biol. 14 (2013) 775–786.
[2] J.A. Olzmann, P. Carvalho, Nat. Rev. Mol. Cell Biol. 20 (2019) 137–155.
[3] Y. Li, D. Munoz-Mayorga, Y. Nie, et al., Cell Metab. 36 (2024) 1351–1370 e1358.
[4] A. Zadoorian, X. Du, H. Yang, Nat. Rev. Endocrinol. 19 (2023) 443–459.
[5] S. Cohen, Int. Rev. Cell Mol. Biol. 337 (2018) 83–110.
[6] A.P. Bailey, G. Koster, C. Guillermier, et al., Cell 163 (2015) 340–353.
[7] M.A. Welte, A.P. Gould, Biochim. Biophys. Acta Mol. Cell Biol. Lipids 1862 (2017) 1260–1272.
[8] E. Jarc, T. Petan, J. Yale, Biol. Med. 92 (2019) 435–452.
[9] T.C. Walther, R.V. Farese Jr., Annu. Rev. Biochem. 81 (2012) 687–714.
[10] C. Dumesnil, L. Vanharanta, X. Prasanna, et al., Nat. Commun. 14 (2023) 915.
[11] C.L. Jackson, Curr. Opin. Cell Biol. 59 (2019) 88–96.
[12] M.E. Pisanu, E. Iorio, F. Facchiano, et al., Int. J. Mol. Sci. 27 (2026) 1715.
[13] K.G. Sprenger, E.E. Lietzke, J.T. Melchior, et al., J. Lipid Res. 66 (2025) 100872.
[14] W.M. Henne, S. Cohen, Nat. Rev. Mol. Cell Biol. 27 (2026) 433–449.
[15] C.M. Fader Kaiser, P.S. Romano, M.C. Vanrell, et al., Front. Cell Dev. Biol. 9 (2021) 826248.
[16] J. Mahamid, D. Tegunov, A. Maiser, et al., Proc. Natl. Acad. Sci. U. S. A. 116 (2019) 16866–16871.
[17] J. Xiang, T. Li, J. Zhang, et al., J. Am. Chem. Soc. 147 (2025) 10724–10736.
[18] S.S. Hussain, T.M. Tran, T.B. Ware, et al., Cell Rep. 36 (2021) 109451.
[19] J. Hartler, H.C. Köfeler, M. Trötzmüller, et al., Sci. Data 1 (2014) 140051.
[20] Q. Qiao, A. Song, G. Jiang, et al., Angew. Chem. Int. Ed. 64 (2025) e202503177.
[21] Y. Zhao, W. Shi, X. Li, et al., Chem. Commun. 58 (2022) 1495–1509.
[22] Z. Li, Q. Qiao, N. Xu, et al., Chin. Chem. Lett. 35 (2024) 108824.
[23] C. Yan, Q. Qiao, W. Zhou, et al., Chin. Chem. Lett. 36 (2025) 110258.
[24] X. Zhou, L. Miao, W. Zhou, Q. Qiao, Z. Xu, Chin. Chem. Lett. 36 (2025) 110984.
[25] P. Greenspan, E.P. Mayer, S.D. Fowler, J. Cell Biol. 100 (1985) 965–973.
[26] B. Qiu, M.C. Simon, Bio Protoc. 6 (2016) e1912.
[27] J. Chen, W. Liu, X. Fang, Q. Qiao, Z. Xu, Chin. Chem. Lett. 33 (2022) 5042–5046.
[28] R. Huang, Q. Qiao, D. Seah, et al., J. Am. Chem. Soc. 147 (2025) 5258–5268.
[29] A. Song, Q. Qiao, N. Xu, et al., Chin. Chem. Lett. 36 (2025) 110643.
[30] N. Xu, Q. Qiao, X. Fang, et al., Anal. Chem. 96 (2024) 4709–4715.
[31] J. Chen, Q. Qiao, H. Wang, et al., Adv. Sci. 11 (2024) 2408030.
[32] X. Fang, Q. Qiao, F. Deng, Z. Xu, Chin. Chem. Lett. 36 (2025) 110980.
[33] W. Bu, X. Guo, X. Lv, et al., Dyes Pigm. 220 (2023) 111735.
[34] Q. Zhang, K. Zhao, X. Tang, et al., Spectrochim. Acta A 321 (2024) 124701.
[35] J. Liu, Y. He, R. Yan, et al., bioRxiv (2025), doi:10.1101/2025.04.03.647137.
[36] R. Zhou, H. Sha, S. Fu, et al., Adv. Sci. 12 (2025) e08792.
[37] S. Lu, Y. Zhao, D. Liu, et al., Anal. Chem. 97 (2025) 4137–4143.
[38] J. Wang, K. Kajiwara, M. Kesherwani, et al., J. Am. Chem. Soc. 147 (2025) 41514–41523.
[39] Q. Qiao, C. Wang, H. Wang, et al., J. Am. Chem. Soc. 147 (2025) 15602–15613.
[40] K. An, Q. Qiao, Lovelesh, et al., Chin. Chem. Lett. 36 (2025) 109786.
[41] J. Li, Q. Qiao, N. Xu, et al., Chin. Chem. Lett. 35 (2024) 108348.
[42] G. Wang, Q. Qiao, W. Jia, et al., Chin. Chem. Lett. 36 (2025) 110130.
[43] T.Le Bahers, C. Adamo, I. Ciofini, J. Chem. Theory Comput. 7 (2011) 2498–2506.
[44] J. Chen, C. Wang, W. Liu, et al., Angew. Chem. Int. Ed. 60 (2021) 25104–25113.
[45] Z. Liu, T. Lu, Q. Chen, Carbon 171 (2021) 514–523.
[46] W. Jiang, J. Chen, K. An, et al., Green Chem. Eng. 4 (2023) 387–392.